AGU PUBLICATIONS

Geophysical Research Letters

RESEARCH LETTER
10.1002/2016GL072079

Key Points:
- Simultaneous oxygen microprofile and current measurements enable the parameterization of turbulent diffusion in the near-sediment boundary layer
- The proposed parameterization provides an estimate of diffusive boundary layer thickness over which molecular diffusion dominates
- A similarity scaling is proposed for near-sediment oxygen microprofiles in stratified natural waters

Supporting Information:
- Supporting Information S1

Correspondence to:
R. Schwefel,
robert.schwefel@epfl.ch

Citation:
Schwefel, R., M. Hondzo, A. Wüest, and D. Bouffard (2017), Scaling oxygen microprofiles at the sediment interface of deep stratified waters, *Geophys. Res. Lett.*, *44*, 1340–1349, doi:10.1002/2016GL072079.

Received 23 NOV 2016
Accepted 26 JAN 2017
Accepted article online 29 JAN 2017
Published online 13 FEB 2017

Scaling oxygen microprofiles at the sediment interface of deep stratified waters

Robert Schwefel[1], Miki Hondzo[2], Alfred Wüest[1,3], and Damien Bouffard[1,3]

[1]Physics of Aquatic Systems Laboratory - Margaretha Kamprad Chair of Environmental Science and Limnology, EPFL, ENAC-IEE-APHYS, Lausanne, Switzerland, [2]Department of Civil, Environmental, and Geo-Engineering, St. Anthony Falls Laboratory, University of Minnesota, Minneapolis, Minnesota, USA, [3]Surface Waters-Research and Management, Swiss Federal Institute of Aquatic Sciences and Technology (Eawag), Kastanienbaum, Switzerland

Abstract Dissolved oxygen microprofiles at the sediment-water interface of Lake Geneva were measured concurrently with velocities 0.25 to 2 m above the sediment. The measurements and scaling analyses indicate dissolved oxygen fluctuations and turbulent fluxes in exceedance of molecular diffusion in the proximity of the sediment-water interface. The measurements allowed the parameterization of the turbulent diffusion as a function of the dimensionless height above the sediment and the turbulence above the sediment-water interface. Turbulent diffusion depended strongly on the friction velocity and differed from formulations reported in the literature that are based on concepts of turbulent and developed wall-bounded flows. The dissolved oxygen microprofiles and proposed parameterization of turbulent diffusion enable a foundation for the similarity scaling of oxygen microprofiles in proximity to the sediment. The proposed scaling allows the estimation of diffusive boundary layer thickness, oxygen flux, and oxygen microprofile distribution in the near-sediment boundary layer.

1. Introduction

Decreasing dissolved oxygen (DO) content of the world's oceans and lakes has gained significant attention in the research community [*Diaz and Rosenberg,* 2008; *Keeling,* 2010; *Bouffard et al.,* 2013; *Donnadieu et al.,* 2016]. The reduction in DO has been attributed to climate change and increased anthropogenic nutrient inputs [*Föllmi,* 2010; *Monteiro et al.,* 2012; *Friedrich et al.,* 2014]. Deoxygenation in deep waters along the bottom boundary layer (BBL) is especially prone to the synergistic effects of climate change, including increasing average water temperature, strength of water column stratification, and accelerated nutrient cycling [*Yoh et al.,* 1983; *Gudasz et al.,* 2010; *Donnadieu et al.,* 2016]. Turbulence above the sediment-water interface (SWI) amplifies DO dynamics, changing the sediment oxygen uptake (SOU) which depends on the supply of the DO fluxes from the BBL to the sediments [*McGinnis et al.,* 2008; *Scalo et al.,* 2013; *Steele et al.,* 2016]. SOU is important for the DO budget in stratified waters, as much of the organic matter decomposition occurs close below the SWI.

Current models for DO depletion typically assume a constant SOU, which is independent of BBL oxygen concentration and dynamics. While this simple approach often provides useful results, it relies on lake-dependent calibration. The inclusion of BBL dynamics in DO depletion models will lead to more realistic parameterizations.

Our objective was to find a similarity scaling for near-sediment DO microprofiles and SOU based on high-resolution (<0.1 mm) DO measurements. Following Fick's first law, DO flux was estimated from the DO gradient and molecular diffusivity [*Jørgensen and Revsbech,* 1985; *Jørgensen and Des Marais,* 1990; *Steinberger and Hondzo,* 1999] in the thin region above the SWI, where molecular diffusion is the dominant transport process. This thin region is called diffusive boundary layer (DBL) with thickness δ_{DBL}. Various field studies have revealed a high dependence of DBL dynamics on BBL currents, which influence δ_{DBL} and the corresponding DO transport to the sediments [*Lorke et al.,* 2003; *Bryant et al.,* 2010a; *Bryant et al.,* 2010b; *Horppila et al.,* 2015].

We measured DO concentration microprofiles at the SWI of Lake Geneva at ~100 and ~130 m depth with 100 μm resolution. Concurrently, velocities were measured close to the SWI from 0.25 to 2.0 m above the bottom in close proximity to the microprofiler. The analysis of the results enabled a similarity scaling of the eddy diffusivity and DO microprofiles above the SWI. The proposed scaling provides (i) the parameterization of turbulent diffusion, (ii) the thickness of the DBL (δ_{DBL}), (iii) the DO flux, and (iv) the DO vertical distribution above the SWI.

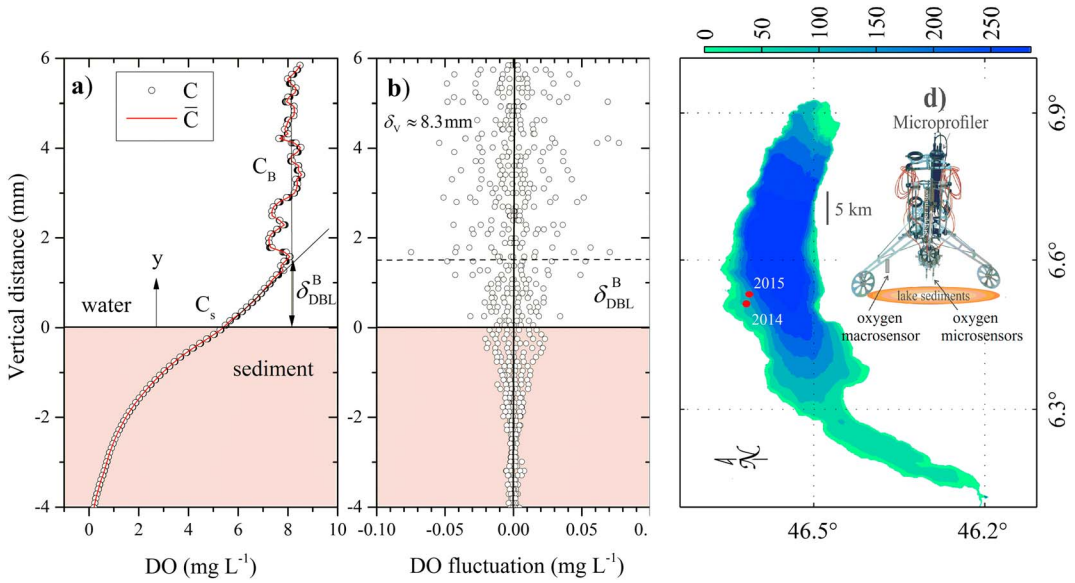

Figure 1. Example of a measured dissolved oxygen (DO) concentration microstructure profile at the sediment-water interface (SWI) of Lake Geneva. (a) The vertical profiles of time-averaged DO concentrations ($\overline{C}$) with a schematic of DO gradient at the SWI (sloped solid line) and bulk DO concentration (C_B, vertical solid line). The intersection of the two solid black lines defines the upper height of the diffusive boundary layer (DBL) thickness (δ^B_{DBL}). The DO fluctuations above the SWI were also observed, e.g., in *Bryant et al.* [2010a] or *Wang et al.* [2016], and are caused by turbulent fluctuations or local inhomogeneities in the DO concentration. (b) The vertical distribution of corresponding instantaneous DO fluctuations ($C' = C - \overline{C}$) with the extent of the viscous sublayer (δ_v) above the sediment. (c) Map of the two Lake Geneva sampling sites in 2014 and 2015 and the depth contours. (d) Photograph of MP4/8 Microprofiler with DO sensors.

2. Materials and Methods

2.1. Study Site

The measurement sites were located in the northern part of Lake Geneva, a deep perialpine lake between France and Switzerland (6.523°E, 46.496°N and 6.519°E, 46.487°N; Figure 1). We report the results of two measurement campaigns with similar instrumentation setups. The first measurement was conducted in July 2014, at a depth of 109 m, and the second in July 2015, at a depth of 133 m (Table 1). At both sites, the bottom slope is ~5%, and the bed contains silty sediments and relatively thin oxic zones in the top few millimeters of the sediment surface.

2.2. Oxygen Microstructure Measurements

Concentrations of DO were quantified using a MP4/8 Microprofiler (Unisense A/S) equipped with Clark-type DO microsensors (Figure 1d). The sensor tip size was ~100 μm with a DO detection limit of 0.01 mg L^{-1}. The spatial resolution of the measurements is of the same size as the sensor tip. An optode (Aanderaa), sampling every 15 s, was positioned outside of the DBL to provide background DO time series during the operations of the MP4/8 Microprofiler. We performed a two-point calibration of the DO microsensors in the field by using the *in situ* data from the optode as the upper reference point and the anoxic sediment as the lower reference point.

During an initial stage of detection, the microsensor was lowered continuously until the DO signal was reduced to 60% of the bulk concentration (C_B) outside the DBL. The reduction of the DO concentration indicated the proximity of the SWI. Afterward, the sensors were raised by ~7 mm and the high-resolution DO microprofile measurements were initiated in steps of 100 μm (precision of motor: 50 μm). The stepper motor stopped for 12 s at each level to ensure steady state conditions. Afterward, six DO measurements were performed at 1.0 Hz sampling rate at the specified depth. The exact position of the SWI was determined from the change in gradient of the measured DO concentration. In addition, analysis of the DO concentration variance provided supporting evidence for the correct position of the SWI.

Table 1. Summary of Measured and Estimated Field Variables[a]

u_* (mm s^{-1})	ε (mm^2 s^{-3})	δ_ν (mm)	η_B (mm)	δ^B_{DBL} (mm)	$\delta^{E_t}_{DBL}$ (mm)	J_w (g m^{-2} d^{-1})	J_{mod} (g m^{-2} d^{-1})	J_s (g m^{-2} d^{-1})
2.2	4.30×10^{-2}	7.5	0.09	1.9	1.0	0.22	0.27	0.21
4.0	2.49×10^{-1}	4.1	0.06	1.9	1.1	0.26	0.32	0.25
1.4	1.07×10^{-2}	11.8	0.12	2.7	1.3	0.13	0.17	0.14
0.7	1.12×10^{-3}	23.6	0.22	4.1	3.3	0.16	0.17	0.16
2.0	3.76×10^{-2}	8.3	0.09	1.7	0.8	0.22	0.20	0.26
2.6	6.83×10^{-2}	6.4	0.08	1.5	0.8	0.18	0.16	0.26
2.2	4.30×10^{-2}	7.5	0.09	1.4	0.9	0.26	0.23	0.29
1.3	1.27×10^{-2}	12.7	0.12	2.1	1.0	0.23	0.25	0.24
1.8	2.33×10^{-2}	9.2	0.10	1.7	1.3	0.29	0.24	0.31
1.0	5.43×10^{-3}	16.5	0.15	2.9	2.2	0.14	0.11	0.18
1.6	1.62×10^{-2}	10.3	0.11	2.4	1.1	0.15	0.18	0.16
1.6	1.75×10^{-2}	10.3	0.11	1.5	1.7	0.27	0.20	0.29
3.3	1.44×10^{-1}	5.0	0.07	1.2	1.1	0.24	0.38	0.20
2.1	3.81×10^{-2}	7.9	0.09	2.1	1.6	0.26	0.32	0.22

[a] u_* is the friction velocity estimated using the 14 Aquadopp current profiles, ε is the rate of energy dissipation in the logarithmic layer [*O'Connor and Hondzo,* 2008], δ_ν is the viscous sublayer thickness, η_B is the Batchelor length scale, δ^B_{DBL} is the DBL thickness based on the bulk DO concentration and the DO gradient at the SWI, and $\delta^{E_t}_{DBL}$ is the DBL thickness estimated based on the exceedance of E_t over 110% of the molecular diffusivity D. J_w is the waterside DO flux to the sediments, and J_s is the sediment-side DO uptake. The kinematic viscosity of lake water at the average temperature of 6°C was $\nu = 1.48$ mm^2 s^{-1}, and the molecular diffusivity of DO was $D = 1.32\times10^{-3}$ mm^2 s^{-1}. The first 12 profiles were measured in 2015, the last two in 2014.

2.3. Current Measurements

An upward looking 2 MHz acoustic Doppler current profiler (ADCP; Nortek Aquadopp) was deployed nearby on the lakebed. Currents were measured in 36 bins of 5 cm size each. The blanking distance, including the height of the instrument frame, was 21.5 cm. This setup enabled a three-dimensional measurement of the current over the vertical distance from ~0.25 to ~2.0 m above the SWI. Data were acquired in burst mode with 1024 samples at 1.0 Hz sampling frequency every 20 min. During the post-processing, the strength of the acoustic signal was verified, and the recorded velocities were time averaged. The distance between the ADCP and the MP4/8 Microprofiler was ~35 m (2015; 12 profiles) and ~100 m (2014; two profiles). Hence, the distance was large enough to exclude interference between the instruments. Systematic deviation in the DO fluctuations with current velocity, which could indicate disturbance from the instruments, was not observed. Recent multibeam bathymetry measurements (the method is presented in *Kremer et al.,* 2015) did not show significant local changes in the bathymetry close to the measurement locations.

2.4. Dissolved Oxygen Microprofile and Fluxes at the Sediment-Water Interface

A conventional method for relating estimates of the waterside DO flux, J_{wD}, to local DO gradients at the SWI is provided by Fick's first law:

$$J_{wD} = -D\frac{dC}{dy}\Big|_{y=0} \tag{1}$$

where D is the molecular diffusion coefficient for DO, C is the DO concentration, y is the vertical distance (Figure 1a), and $\frac{dC}{dy}\big|_{y=0}$ is the local DO gradient at the SWI. Similarly, in the water column, further away from the SWI, the turbulent DO flux, J_{wE}, is estimated by

$$J_{wE} = -E\frac{d\overline{C}}{dy}\Big|_{y} \tag{2}$$

where E is the turbulent diffusion coefficient for DO transport at distance y and $\overline{C}$ is the time-averaged DO concentration. The total DO flux, J_w, is the sum of molecular and turbulent diffusion processes, which are defined analogous to Fick's first law as

$$J_w = -(D+E)\frac{d\overline{C}}{dy} = -E_t\frac{d\overline{C}}{dy} \tag{3}$$

where $E_t = D + E$ is the total diffusion coefficient.

In the absence of significant DO sinks in the DBL, J_{wD} and J_w are equal. Above the DBL, the ratio of the concentration gradients defines E_t/D [*Higashino et al.,* 2008]:

$$\frac{E_t}{D} = \frac{\frac{df}{dy}\big|_{y=0}}{\frac{df}{dy}\big|_{y}} \tag{4}$$

where $f = \frac{\overline{C}-\overline{C}_S}{\overline{C}_B-\overline{C}_S}$ is the DO concentration similarity group with $\overline{C}_S$ as the time-averaged concentration at the SWI and $\overline{C}_B$ as the time-averaged bulk concentration in the BBL [*Steinberger and Hondzo,* 1999].

In turbulent wall-bounded flows, the nondimensional vertical distance reads $y^+ = \frac{y\,u_*}{\nu}$, where u_* is the friction velocity (Figure S1 in the supporting information) and ν is the kinematic viscosity. Defining a nondimensional DO concentration by

$$C^+ = \frac{(\overline{C} - \overline{C}_S)\,u_*}{J_w} \tag{5}$$

we can integrate equation (3) (see Supporting Information, Text S1) and obtain at height $y^{+'}$

$$C^+ = -\int_0^{y^{+'}} \frac{dy^+}{\frac{1}{S_c} + \frac{E}{\nu}} \tag{6}$$

where $S_c = \nu/D$ is the Schmidt number [*Dade*, 1993; *Hondzo et al.,* 2005]. To derive a scaling expression for C^+ against y^+, a functional dependence of E_t/ν versus y^+ is required. We conducted field measurements to quantify DO microprofiles, currents, and u_* and subsequently develop the functional relationship between E_t/ν and the vertical distance above the SWI.

3. Results and Discussion

3.1. Current Measurements

Figure S1 represents longitudinal time-averaged vertical velocity profiles, starting with the first bin ~0.25 m above the SWI. Each symbol depicts a time-averaged velocity over one burst of 1024 s. The average thickness of the BBL, the height at which $\bar{u} = 0.99\,\bar{u}_{max}$, with $\bar{u}_{max}$ being the maximum velocity over the measured profile, was ~1.7 m. The overall depth-averaged longitudinal velocity was 0.017 m s^{-1} with the maximum of 0.030 m s^{-1}. In the proximity of the SWI, the longitudinal velocities followed most of the time the turbulent log-law velocity profile, typical for a smooth bed, with $\frac{\bar{u}}{u_*} = \frac{1}{\kappa}\ln\left(\frac{y\,u_*}{\nu}\right) + B$ (Figure S1), where κ is the von Kármán constant and B is an additive constant. The slope of the longitudinal velocity against ln(y^+) with the coefficient of determination >95% were used to estimate u_* for the depicted velocity profiles (Table 1). For very low flows, velocity profiles did not follow the log law [*Lorke et al.,* 2002], which occurred particularly often during the first measurement campaign. Those measurements were omitted in this study. Using the averaged longitudinal velocity and BBL thickness, the Reynolds number was approximately 20,000 indicating turbulent conditions. *Lorke et al.* [2002] showed that logarithmic velocity profiles were not observed for velocities below 1 cm s^{-1}, which was never the case in the profiles used in this study. The viscous sublayer thickness at the SWI, $\delta_\nu \approx 11\,\frac{\nu}{u_*}$ [*Wüest and Lorke,* 2003], ranged from 4 to 23 mm (Table 1). Due to the 21.5 cm blanking distance of the ADCP, the current measurements do not include the region of the viscous sublayer. With a friction velocity of $u_* \approx 3$ mm s^{-1}, however, it takes only about 5 min for currents at a distance of ~1 m above the SWI to adjust to local sediment roughness. Since the ADCP measurements were averaged over one burst (1024 s; averaging over two bursts or only 600 s did not change the results significantly), u_* calculated from measured velocity gradients is a good estimate of turbulence close to the SWI. δ_ν was significantly larger than the grain size of the sediment (typically ~0.05 mm), which justified the smooth bed assumption for the SWI.

The time-averaged longitudinal velocity was approximately logarithmic from a minimum vertical distance of $y^+ = 140$ to the maximum distance of $y^+ = 4000$. The minimum vertical distance of the log layer to the SWI was consistent with the condition of $y^+ > 30$, typical for turbulent wall-bounded flows [*George,* 2007]. The deviation from logarithmic behavior at maximum vertical distance was observed at an average distance of about $y^+ = 1800$. The flow was not fully developed; rather, it experienced acceleration and deceleration phases as typical for geophysical BBL flows [*Lorke et al.,* 2003; *Scalo et al.,* 2013]. Low bottom velocities governed by

the Poincaré waves with a period of ~10 h were detected. The existence of logarithmic velocity profiles, which are triggered by internal Poincaré and Kelvin waves in Lake Geneva, is in accordance with the field measurements of *Bouffard and Lemmin* [2013]. The analyses of spectral densities of longitudinally fluctuating velocities in the logarithmic region depicted the "5/3" inertial subrange over periods from 5 to 100 s and indicated turbulent flow in the proximity of the sediment.

3.2. Oxygen Microprofiles

Fourteen DO microprofiles were collected for different flows above the SWI under log-law conditions. For each profile, the SWI was located from the change in the DO gradient due to the different diffusion coefficients in the water and sediment [*Røy et al.,* 2004]. The position of the SWI was set to $y = 0$. Figure 1a depicts a typical measured DO microprofile. Other examples are shown in Figure S2. In the water column above the SWI ($y > 3$ mm), time-averaged DO concentration profiles ($\overline{C}$) were almost constant. Although well below the upper height of the viscous sublayer ($\delta_\nu \approx 8.3$ mm) the instantaneous DO concentrations (C) showed fluctuations. These fluctuations ($C' = C - \overline{C}$) with an absolute magnitude of up to 0.08 mg L^{-1} and a standard deviation of 0.01 to 0.03 mg L^{-1} above the SWI indicated appreciable high-frequency fluctuations in the DBL (Figure 1b). In the very proximity of the SWI ($y < 2$ mm), $\overline{C}$ decreased toward the sediments due to the DO consumption in the sediments. In this region, the time-averaged DO profile approaches a straight line and intersects the bulk time-averaged DO concentration ($\overline{C}_B$) at the vertical distance δ^B_{DBL} from the SWI. The δ^B_{DBL} provides a basis for the customary estimation of waterside DO flux (1), which can be approximated by $J_{wD} \approx -\frac{D}{\delta^B_{DBL}}\left(\overline{C}_B - \overline{C}_S\right)$ at the SWI. The fundamental premise of the flux estimation is that the DO concentration gradient at the SWI (equation (1)) is accurately estimated by $\frac{dC}{dy}|_{y=0} \approx \frac{\left(\overline{C}_B - \overline{C}_S\right)}{\delta^B_{DBL}}$, whereas molecular diffusion is the dominant transport mechanism of DO. However, fluctuations of DO were consistently detected within δ^B_{DBL} in all field data (Figure 1b). A distinct fluctuation maximum at the SWI, reported by *Røy et al.* [2004] in laboratory experiments, was not observed. Instead, C' remained high above δ^B_{DBL} and decreased within the DBL. The source of these fluctuations might be turbulent transport in proximity to the DBL or lateral variability of DO concentration above the DBL which is transported downward toward the SWI. The increase in turbulent diffusion (see section 3.3) very close to the DBL is, however, an indication of turbulent transport processes. Nonlinear concentration gradients close to the SWI were also reported in several other studies [*Nishihara and Ackerman*, 2007; *Hondzo et al.,* 2005; *O'Connor and Hondzo*, 2008]. Below, the SWI ($y < -1$ mm), the DO fluctuations were reduced to the precision of the DO sensors (~0.01 mg L^{-1}).

3.3. Power Law Scaling

The DO concentration microprofiles and equation (4) provided the basis for estimating diffusion coefficients at the SWI (Figure 2a). The profiles were fit with a third degree polynomial ($R^2 > 0.85$ and with three exceptions $R^2 > 0.98$), and its derivative at height y and height 0 were used to determine $\frac{E_t}{D} = \frac{\frac{df}{dy}|_{y=0}}{\frac{df}{dy}|_y}$. Values of E_t were determined precisely in the DBL and in the lower transition zone above the DBL but not reliably further above since the change in DO concentration due to natural fluctuations became too high. The customary approach to scaling is to seek a functional relationship E_t/ν versus y^+ [*Van Driest,* 1956; *Shaw and Hanratty,* 1977; *Dade,* 1993]. Figure 2a displays considerable variability of E_t/ν against y^+ and lacks of similarity of profiles for different flows. The vertical scale on the right y axis shows the equivalent E_t/D variability and indicates that the total diffusion exceeds the molecule already at $y^+ < 3$ in the majority of profiles (Figure 2a, horizontal dotted line). The reported parameterizations of E_t/ν were found under laboratory conditions for developed turbulent flows, which do not necessarily hold under field conditions in stratified waters. Near the SWI of developed flows, E_t/ν scales as y^{+4} [*Van Driest,* 1956] or $E_t/\nu \sim y^{+3}$ [*Dade,* 1993]. To account for the modulating effects of developing flows, a parameterization of E_t/ν versus "stretched" wall units, $\alpha_c y^+$, was investigated (Figure 2b). The constant α_c was selected for each profile of E_t/ν so that E_t/ν scales universally with $\alpha_c y^+$. α_c was of the order of 1 and had a strong functional dependence on the Reynolds number ($\mathrm{Re}_{\eta_B} = \frac{u_* \eta_B}{\nu}$), which is based on u_* and the Batchelor microscale ($\eta_B = \left(\frac{\nu D^2}{\varepsilon}\right)^{1/4}$). The energy dissipation, ε, was determined by using the log law estimation, $\varepsilon \sim \frac{u_*^3}{\kappa y}$, averaged over the logarithmic region of the corresponding velocity

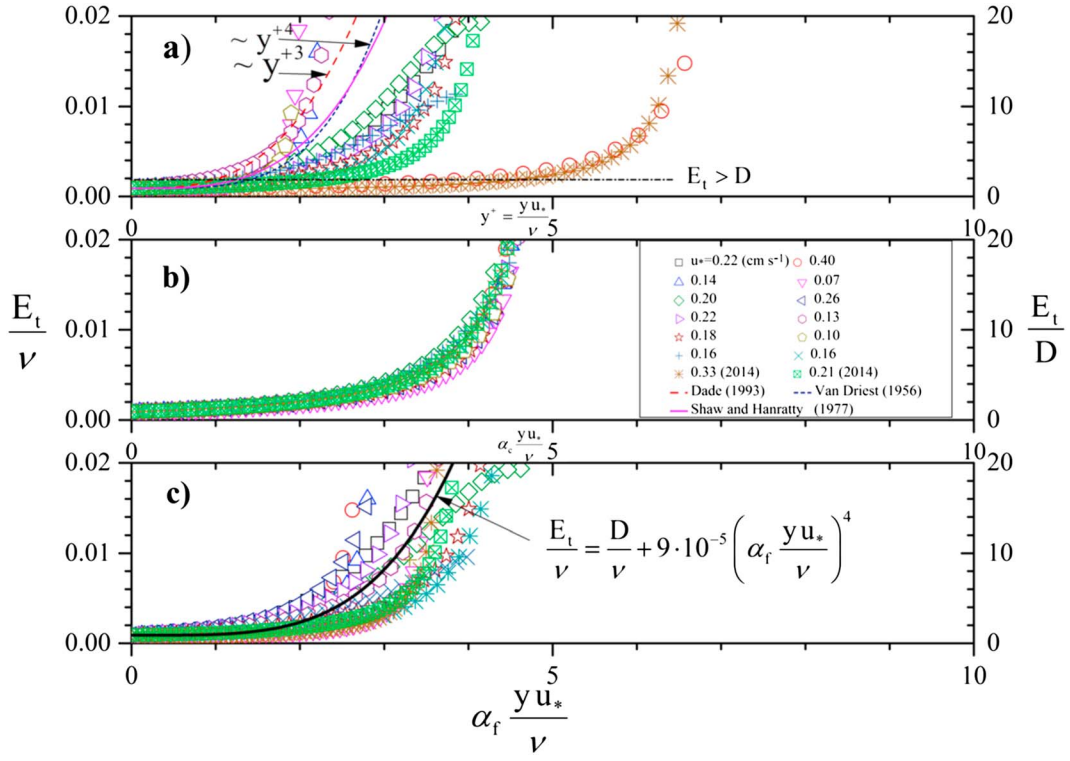

Figure 2. Dimensionless total diffusion (molecular and eddy) coefficient (E_t/ν) variability against the dimensionless vertical distance above the SWI. (a) The traditional scaling of E_t/ν against the wall units $y^+ = \frac{y u_*}{\nu}$. The data are compared to three parameterizations used in the literature. (b) E_t/ν against the stretched wall units, $\alpha_c y^+$, where α_c is a constant (order ~1), different for each profile of E_t/ν. (c) E_t/ν against the predicted wall units, $\alpha_f y^+$, where $\alpha_f = 16 \cdot \exp\left(-21 \cdot Re_{\eta_B}\right)$. $Re_{\eta_B} = \frac{u_* \eta_B}{\nu}$ is the Reynolds number defined by the Batchelor length scale ($\eta_B = \left(\frac{\nu D^2}{\varepsilon}\right)^{1/4}$, where D is the molecular DO diffusion coefficient and ε is the energy dissipation rate).

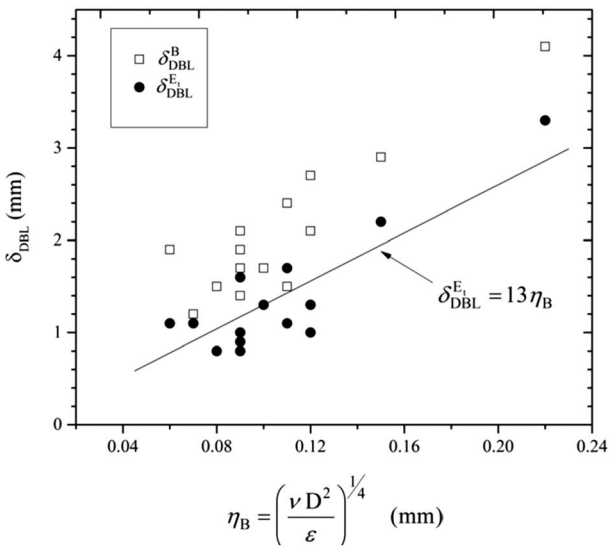

Figure 3. Dependence of DBL thickness on Batchelor scale at which DO fluctuations are smoothened by molecular diffusion. δ^B_{DBL} is the DBL thickness based on the bulk DO concentration and local time-averaged micro-oxygen concentration gradient at the SWI, and $\delta^{E_t}_{DBL}$ is the DBL thickness over which molecular diffusion dominates at the SWI.

profiles [*O'Connor et al.*, 2009] (Table 1). The choice of another expression for ε, e.g., closer to the sediment depth [*Lorke et al.*, 2003; *Inoue et al.*, 2008], would not change the proportionality of α_c to u_*^3. A fit of α_c as a function of Reynolds number resulted in $\alpha_f = 16 \cdot \exp\left(-21 \cdot Re_{\eta_B}\right)$, which explained 85% of the variability of α_c (Figure S3). The new parameterization E_t/ν versus $\alpha_f y^+$ is depicted in Figure 2c. The scaling relationship $E_t/\nu \sim (\alpha_f y^+)^4 \sim \left(16 \cdot \exp\left(-21 \cdot Re_{\eta_B}\right) \cdot y^+\right)^4$ (Figure 2c) suggests that the total diffusivity has abrupt variations within the DBL and is much less pronounced in the developed flows far outside the DBL. The sharp increase in the dispersive transport of DO (including total diffusive transport and additional advective transport which scales with u_*) causes apparent variability in DO microprofiles, which is depicted by the varying slopes in the transition region from DBL to C_B

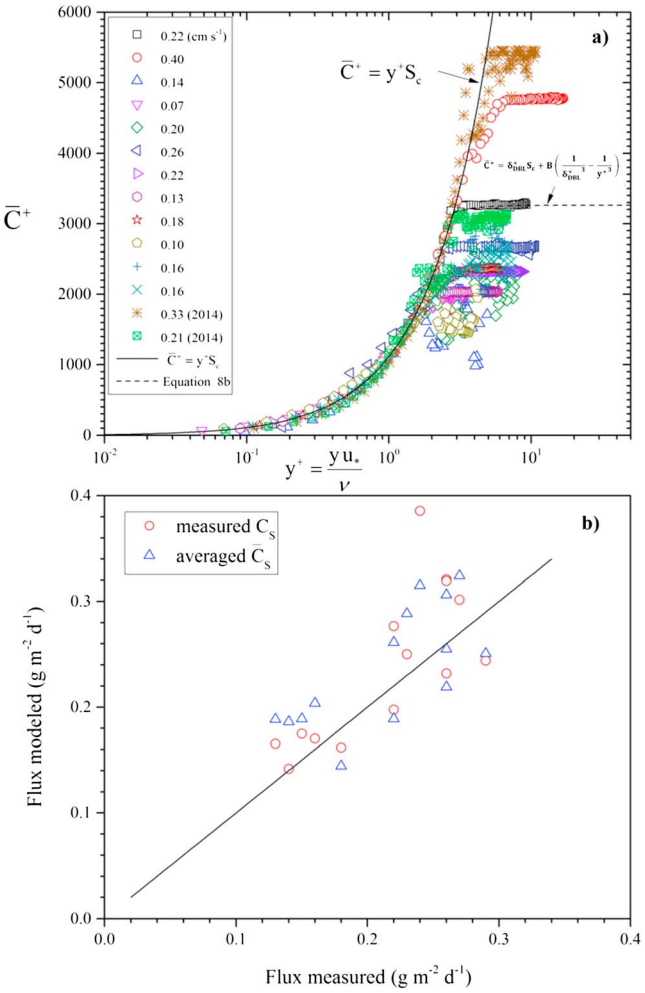

Figure 4. (a) Measured and predicted near-sediment profiles of the dimensionless DO concentration ($C^+ = \frac{(\overline{C}-C_s)\,u_*}{J_w}$). The proposed scaling relationships are depicted within the DBL ($\overline{C}^+ = y^+ S_c;\ \ \delta^+_{DBL} > y^+ > 0$) and in the water column above the DBL ($\overline{C}^+ = \delta^+_{DBL} S_c + B\left(\frac{1}{\delta^+_{DBL}3} - \frac{1}{y^{+3}}\right);\ y^+ \geq \delta^+_{DBL}$). S_c is the Schmidt number, $\delta^+_{DBL} = \frac{\delta^{E_t}_{DBL}\,u_*}{\nu}$ is the dimensionless DBL thickness with $\delta^{E_t}_{DBL}$ as defined in section 3.3, and $B = 0.05 \cdot \exp\left(84 \cdot Re_{\eta_B}\right)$. $Re_{\eta_B} = \frac{u_* \eta_B}{\nu}$ is the Reynolds number defined by the Batchelor scale. (b) Flux of DO into the sediment calculated by equations (8a) and (8b) using δ^+_{DBL} calculated by equation (7) as a function of the measured fluxes J_W. The circles show the results using the measured DO concentration at the sediment as C_S, and for the triangles, the time-averaged sediment DO concentration $\overline{C}_S$ is used. The 1:1 black line indicates equal fluxes. The coefficient of determination between the measured and estimated flux was 70% for the measured C_S and 75% for the time-averaged $\overline{C}_S$.

(Figure 1a). We have observed similar transition patterns in several vertical microstructure DO profiles of Lake Geneva and other lakes [*Bryant et al.*, 2010a, 2010b].

δ_{DBL} was estimated from the measured DO microprofiles following the above-described conventional approach of *Jørgensen and Revsbech* [1985], based on the local time-averaged DO gradient at the SWI and the bulk DO concentration in the water column (Table 1, δ^B_{DBL}). The thickness δ^B_{DBL} ranged from 1.2 to 4.1 mm. In addition, we defined $\delta^{E_t}_{DBL}$ as the layer at which E_t exceeds D by 10%, indicating the region in which molecular diffusion is dominant. The estimates of $\delta^{E_t}_{DBL}$ are provided in Table 1. The thickness ranged from 0.8 to 3.3 mm. The average of δ^B_{DBL} was 50% larger than the corresponding $\delta^{E_t}_{DBL}$. Figure 3 displays the functional dependence of $\delta^{E_t}_{DBL}$ and δ^B_{DBL} versus the Batchelor scale η_B. We observe a linear increase of $\delta^{E_t}_{DBL}$ against the Batchelor scale, with the coefficient of determination 76%, as described by

$$\frac{\delta^{E_t}_{DBL}}{\eta_B} = 13 \qquad (7)$$

Equation (7) allows to estimate the DBL thickness solely based on current measurements. A similar functional dependence of δ^B_{DBL} on η_B was suggested by *Lorke et al.* [2003]. The vertical extent of "y" was considered in the region with the log-law velocity distribution. The proposed functional relationship of E_t/ν versus y^+ was substituted into equation (6), the integral was split into the region with dominance of molecular diffusion and the region with dominance of turbulent diffusion, and upon integration, the following scaling expression for the distribution of DO with distance from the SWI was obtained (see Supporting Information, Text S1):

$$\overline{C}^+ = y^+ S_c \quad \delta^+_{DBL} > y^+ > 0 \qquad (8a)$$

$$\overline{C}^+ = \delta^+_{DBL} S_c + B\left(\frac{1}{\delta^+_{DBL}3} - \frac{1}{y^{+3}}\right) \qquad y^+ \geq \delta^+_{DBL} \qquad (8b)$$

where $B = 0.05\ \exp\left(84Re_{\eta_B}\right)$ and $\delta^{+}_{\mathrm{DBL}} = \frac{\delta^{E_t}_{\mathrm{DBL}}\, u_*}{\nu}$ with $\delta^{E_t}_{DBL}$ defined as the thickness at which E_t exceeds D by 10%. In Figure 4a the measured DO profiles are compared to the proposed scaling (equations (8a) and (8b)). Within δ^{+}_{DBL}, the data are universally scaled by equation (8a) and indicate that the slope of $\left(\overline{C} - \overline{C}_s\right)$ versus y provides the estimate of waterside DO flux (J_w). An estimate of sediment-side DO uptake (J_s) was determined by the in situ microstructure sediment data (Figure 1a) and the algorithm proposed by *Berg et al.* [1998]. The very porous first millimeter of the sediment was parameterized with a porosity of $\phi = 0.98$ and set to $\phi = 0.90$ below in the sediment [e.g., *Bryant et al.,* 2010b]. The diffusivity in the sediment (D_S) was calculated as $D_S = \phi D$ [*Bryant et al.,* 2010b]. Bioirrigation and oxygen production was assumed to be negligible in the sediment. The two independent estimates of J_w and J_s were similar, confirming our estimate of J_w and indicating quasi steady state flux conditions under which J_w was balanced by the corresponding J_s within the sediment (Table 1). An average time scale over which DO was transported across $\delta^{E_t}_{\mathrm{DBL}}$ by molecular diffusion was $\frac{\left(\delta^{E_t}_{\mathrm{DBL}}\right)^2}{D} \sim 20$ min and close to the total duration of sampling DO and currents in the field. Outside the DBL ($y^{+} > \delta^{+}_{\mathrm{DBL}}$), the proposed scaling (equation (8b)) described the data well (Figure 4a). One example of the proposed scaling and comparison with the data is depicted by the dotted black line.

Researchers often face the challenging questions on how to estimate J_w and DBL based on limited DO data. The proposed DO scaling (8b) has two free parameters (J_w and δ^{+}_{DBL}) for given u_* and enables an estimate of the parameters by the limited DO data outside the δ^{+}_{DBL}. Furthermore, using equation (7) to estimate δ^{+}_{DBL} and equation (8b) to calculate C^{+} based solely on current data, $J_{\mathrm{mod}} = \frac{\left(\overline{C} - C_S\right)u_*}{C^{+}}$ can then be determined only from the DO concentration in the region with dominance of turbulent diffusion and C_S. Using the measured values of C_S, the modeled DO fluxes were very close to those derived from the measured microprofiles (Table 1). For an accurate description of the DO concentration at the SWI, the biological conditions at the sediment surface have to be considered. Monod's kinetic model can be implemented to describe microbial growth and associated oxygen uptake in the sediment to calculate C_S [*Nakamura and Stefan,* 1994; *Higashino et al.,* 2008]. However, even if the variation in C_S is neglected and a time-averaged concentration at the sediment surface is assumed instead, the observed fluxes are still close to the measured ones (Figure 4b) since the variability in the DO profiles is larger above the SWI than in the sediment [*Scalo et al.,* 2013]. Based on current data only, the proposed scaling is appropriate to the modeling of DO microprofiles and provides a description of the physical control of SOU. The directly measured rates of sediment oxygen uptake and those estimated from equations (7) and (8a) and (8b) are depicted in Figure 4b.

4. Conclusions

Simultaneous DO microprofile and ADCP measurements were performed in the BBL in the hypolimnion of Lake Geneva. The velocity profiles revealed, despite low (2 to 3 cm s^{-1}) currents, a turbulent flow with log layer characteristics, and traditionally estimated DBL thickness of 1.2 to 4.1 mm. However, the submillimeter-scale DO profile measurements demonstrated concentration fluctuations even within the DBL, where the conventional approach advocates molecular diffusion as dominant mechanism of DO flux to the sediments. Estimations of eddy diffusivity in proximity to the SWI showed that commonly used scaling functions derived under developed flow conditions do not apply for stratified natural waters and that eddy diffusion plays an important role for the DO transport close to the SWI. Accurate flux estimation based on measured DO concentration profiles depends on adequate measurement of spatial resolution. Similar findings were reported for the estimates of heat flux through the double-diffusively convective layers in Lake Kivu. Estimating the fluxes in the molecular center of the interfaces [*Sommer et al.,* 2013] provided 5 times larger values than a linear fit across the entire interfaces [*Schmid et al.,* 2010], which are "contaminated" by turbulent fluctuations. Therefore, the risk of underestimating molecular fluxes applies to any turbulent-molecular transition region.

A new functional relationship between E_t/ν and the dimensionless height above the sediment was established based on the field data. E_t was not only proportional to y^{+n}. Instead, a factor depending on the turbulence above the SWI was necessary to obtain a scaling parameterization for eddy diffusivity. Based on this study, it is not possible to determine if this is a general phenomenon for low-turbulence conditions or caused by the dominant forcing by basin-scale internal waves typical for Lake Geneva. Using the relationship

between E_t and u_*, a universal scaling law for C^+ can be derived. δ_{DBL} was shown to be dependent on the turbulence conditions in the BBL above the SWI. Based on this dependence and the universal scaling law (equations (8a) and (8b)), sediment oxygen uptake can be determined solely from hydrodynamic conditions close to the sediment and DO concentrations at the sediment surface. This result will facilitate DO depletion estimates and improve the practical parameterization of DO fluxes to the sediment in numerical modeling, where the impact of BBL hydrodynamics on sediment oxygen uptake is still largely neglected.

Acknowledgments
This work has been developed during the sabbatical leave of M. Hondzo to EPFL, and we acknowledge the financial contribution by the ENAC Visiting Professor Program. We are thankful to the excellent collaboration with Lee Bryant (University of Bath), Beat Müller and Thomas Steinsberger (both Eawag), and Sébastien Lavanchy (EPFL). The first author was supported by the Swiss National Science Foundation grants 200021-146652 and 200020-165517. Field data can be accessed by the corresponding author.

References

Berg, P., N. Risgaard-Petersen, and S. Rysgaard (1998), Interpretation of measured concentration profiles in sediment pore water, *Limnol. Oceanogr.*, *43*(7), 1500–1510, doi:10.4319/lo.1998.43.7.1500.
Bouffard, D., and U. Lemmin (2013), Kelvin waves in Lake Geneva, *J. Great Lakes Res.*, *39*, 637–645, doi:10.1016/j.jglr.2013.09.005.
Bouffard, D., D. J. Ackerman, and L. Boegman (2013), Factors affecting the development and dynamics of hypoxia in a large shallow lake: Hourly to seasonal patterns, *Water Resour. Res.*, *49*, 2380–2394, doi:10.1002/wrcr.20241.
Bryant, L. D., C. Lorrai, D. F. McGinnis, A. Brand, A. Wüest, and J. C. Little (2010a), Variable sediment oxygen uptake in response to dynamic forcing, *Limnol. Oceanogr.*, *55*, 950–964, doi:10.4319/lo.2010.55.2.0950.
Bryant, L. D., D. F. McGinnis, C. Lorrai, A. Brand, J. C. Little, and A. Wüest (2010b), Evaluating oxygen fluxes using microprofiles from both sides of the sediment-water interface, *Limnol. Oceanogr. Meth.*, *8*, 610–627, doi:10.4319/lom.2010.8.0610.
Dade, W. B. (1993), Near-bed turbulence and hydrodynamic control of diffusional mass transfer at the sea floor, *Limnol. Oceanogr.*, *38*(1), 52–69, doi:10.4319/lo.1993.38.1.0052.
Diaz, J. R., and R. Rosenberg (2008), Spreading dead zones and consequences for marine ecosystems, *Science*, *321*, 926–929, doi:10.1126/science.1156401.
Donnadieu, Y., E. Pucéat, M. Moiroud, F. Guillocheau, and J.-F. Deconinck (2016), A better-ventilated ocean triggered by Late Cretaceous changes in continental configuration, *Nat. Commun.*, *7*, 10316, doi:10.1038/ncomms10316.
Föllmi, K. B. (2010), Early Cretaceous life, climate and anoxia, *Cretaceous Res.*, *35*, 230–257, doi:10.1016/j.cretres.2011.12.005.
Friedrich, J., et al. (2014), Investigating hypoxia in aquatic environments: Diverse approaches to addressing a complex phenomenon, *Biogeosciences*, *11*(4), 1215–1259, doi:10.5194/bg-11-1215-2014.
George, W. K. (2007), Is there a universal log law for turbulent wall-bounded flows?, *Phil. Trans. R. Soc. A*, *365*, 789–806, doi:10.1098/rsta.2006.1941.
Gudasz, C., D. Bastviken, K. Steger, K. Premke, S. Sobek, and L. J. Tranvik (2010), Temperature-controlled organic carbon mineralization in lake sediments, *Nature*, *466*(7305), 478–481, doi:10.1038/nature09186.
Higashino, M., B. L. O'Connor, M. Hondzo, and H. G. Stefan (2008), Oxygen transfer from flowing water to microbes in an organic sediment bed, *Hydrobiologia*, *614*, 219–231, doi:10.1007/s10750-008-9508-8.
Hondzo, M., T. Feyaerts, R. Donovan, and B. L. O'Connor (2005), Universal scaling of dissolved oxygen distribution at the sediment-water interface: A power law, *Limnol. Oceanogr.*, *50*(5), 1667–1676, doi:10.4319/lo.2005.50.5.1667.
Horppila, J., P. Köngäs, J. Niemistö, and S. Hietanen (2015), Oxygen flux and penetration depth in the sediments of aerated and non-aerated lake basins, *Int. Rev. Hydrobiol.*, *100*, 106–115, doi:10.1002/iroh.201401781.
Inoue, T., Y. Nakamura, and M. Sayama (2008), A new method for measuring flow structure in the benthic boundary layer using an acoustic Doppler velocimeter, *J. Atmos. Oceanic Tech.*, *25*, 822–830, doi:10.1175/2007JTECHO531.1.
Jørgensen, B. B., and D. J. Des Marais (1990), The diffusive boundary layer of sediments: Oxygen microgradients over a microbial mat, *Limnol. Oceanogr.*, *35*(6), 1343–1355, doi:10.2307/2837444.
Jørgensen, B. B., and N. P. Revsbech (1985), Diffusive boundary layers and the oxygen uptake of sediments and detritus, *Limnol. Oceanogr.*, *30*(1), 111–122, doi:10.2307/2836220.
Keeling, F., R. Körtzinger, and N. Gruber (2010), Ocean deoxygenation in a warming world, *Ann. Rev. Mar. Sci.*, *2*, 199–229, doi:10.1146/annurev.marine.010908.163855.
Kremer, K., M. Hilbe, G. Simpson, L. Decrouy, W. Wildi, and S. Girardclos (2015), Reconstructing 4000 years of mass movement and tsunami history in a deep peri-Alpine lake (Lake Geneva, France-Switzerland), *Sedimentology*, *62*, 1305–1327, doi:10.1111/sed.12190.
Lorke, A., L. Umlauf, T. Jonas, and A. Wüest (2002), Dynamics of turbulence in low-speed oscillating bottom-boundary layers of stratified basins, *Environ Fluid Mech*, *2*(4), 291–313, doi:10.1023/A:1020450729821.
Lorke, A., B. Müller, M. Maerki, and A. Wüest (2003), Breathing sediments: The control of diffusive transport across the sediment-water interface by periodic boundary-layer turbulence, *Limnol. Oceanogr.*, *48*(6), 2077–2085, doi:10.2307/3597808.
McGinnis, D. F., P. Berg, A. Brand, C. Lorrai, T. J. Edmonds, and A. Wüest (2008), Measurements of eddy correlation oxygen fluxes in shallow freshwaters: Towards routine applications and analysis, *Geophys. Res. Lett.*, *35*, L04403, doi:10.1029/2007GL032747.
Monteiro, F. M., R. D. Pancost, A. Ridgwell, and Y. Donnadieu (2012), Nutrients as the dominant control on the spread of anoxia and euxinia across the Cenomanian-Turonian oceanic anoxic event (OAE2): Model-data comparison, *Paleoceanography*, *27*, PA4209, doi:10.1029/2012PA002351.
Nakamura, Y., and H. Stefan (1994), Effect of flow velocity on sediment oxygen demand: Theory, *J. Environ. Eng.*, *120*(5), 996–1016, doi:10.1061/(ASCE)0733-9372(1994)120:5(996).
Nishihara, G. N., and J. D. Ackerman (2007), On the determination of mass transfer in a concentration boundary layer, *Limnol. Oceanogr. Methods*, *5*, 88–96, doi:10.4319/lom.2007.5.88.
O'Connor, B. L., and M. Hondzo (2008), Dissolved oxygen transfer to sediments by sweep and eject motions in aquatic environments, *Limnol. Oceanogr.*, *53*, 566–578, doi:10.4319/lo.2008.53.2.0566.
O'Connor, L. B., M. Hondzo, and J. W. Harvey (2009), Incorporating both physical and kinetic limitations in quantifying dissolved oxygen flux to aquatic sediments, *J. Enviro. Eng-ASCE*, *135*, 1304–1314, doi:10.1061/(ASCE)EE.1943-7870.0000093.
Røy, H., M. Huettel, and B. B. Jørgensen (2004), Transmission of oxygen concentration fluctuations through the diffusive boundary layer overlying aquatic sediments, *Limnol. Oceanogr.*, *49*, 686–692, doi:10.4319/lo.2004.49.3.0686.
Scalo, C., L. Boegman, and U. Piomelli (2013), Large-eddy simulation and low-order modeling of sediment-oxygen uptake in a transitional oscillatory flow, *J. Geophys. Res. Oceans*, *118*, 1926–1939, doi:10.1002/jgrc.20113.
Schmid, M., M. Busbridge, and A. Wüest (2010), Double-diffusive convection in Lake Kivu, *Limnol. Oceanogr.*, *55*, 225–238, doi:10.4319/lo.2010.55.1.0225.

Shaw, D. A., and J. Hanratty (1977), Turbulent mass transfer rates to a wall for large Schmidt numbers, *AIChE J.*, *23*, 28–37, doi:10.1002/aic.690230106.

Sommer, T., J. R. Carpenter, M. Schmid, R. G. Lueck, M. Schurter, and A. Wüest (2013), Interface structure and flux laws in a natural double-diffusive layering, *J. Geophys. Res. Oceans*, *118*, 6092–6106, doi:10.1002/2013JC009166.

Steele, E. C. C., W. Alex, M. Nimmo-Smith, and A. Vlasenko (2016), Direct measurement of hairpin-like vortices in the bottom boundary layer of the coastal ocean, *Geophys. Res. Lett.*, *43*, 1175–1183, doi:10.1002/2015GL067148.

Steinberger, N., and M. Hondzo (1999), Diffusional mass transfer at sediment-water interface, *J. Enviro. Eng-ASCE*, *125*(2), 192–200, doi:10.1061/(ASCE)0733-9372(1999)125:2(192).

Van Driest, E. R. (1956), On turbulent flow near a wall, *J. Aero-Nautical Sci.*, *23*, 1007–1019, doi:10.2514/8.3713.

Wang, J., L. Zhao, R. Fan, and H. Wei (2016), Scaling relationships for diffusive boundary layer thickness and diffusive flux based on in situ measurements in coastal seas, *Prog. Oceanogr.*, *144*, 1–14, doi:10.1016/j.pocean.2016.03.001.

Wüest, A., and A. Lorke (2003), Small-scale hydrodynamics in lakes, *Annu. Rev. Fluid Mech.*, *35*(1), 373–412, doi:10.1146/annurev.fluid.35.101101.161220.

Yoh, M., H. Terai, and Y. Saijo (1983), Accumulation of nitrous oxide in the oxygen deficient layer of freshwater lakes, *Nature*, *301*, 327–329, doi:10.1038/301327a0.